

Finding pathways for stoichiometric Co₄N thin films

Nidhi Pandey¹, Mukul Gupta^{1*}, Rachana Gupta², Zaineb Hussain¹, V. R. Reddy¹, D. M. Phase¹ and Jochen Stahn³

¹UGC-DAE Consortium for Scientific Research, University Campus, Khandwa Road, Indore 452 001, India

²Institute of Engineering and Technology DAVV, Khandwa Road, Indore 452 017, India and

³Laboratory for Neutron Scattering and Imaging,

Paul Scherrer Institut, CH-5232 Villigen PSI, Switzerland

* Corresponding author email: mgupta@csr.res.in

(Dated: January 15, 2019)

In this work, we studied the pathways for formation of stoichiometric Co₄N thin films. Polycrystalline and epitaxial Co₄N films were prepared using reactive direct current magnetron (dcMS) sputtering technique. A systematic variation in the substrate temperature (T_s) during the dcMS process reveals that the lattice parameter (LP) decreases as T_s increases. We found that nearly stoichiometric Co₄N films can be obtained when $T_s = 300$ K. However, they emerge from the transient state of Co target ($\phi 3$ inch). By reducing the target size to $\phi 1$ inch, now the Co₄N phase formation takes place from the metallic state of Co target. In this case, LP of Co₄N film comes out to be $\sim 99\%$ of the value expected for Co₄N. This is the largest value of LP found so far for Co₄N. The pathways achieved for formation of polycrystalline Co₄N were adopted to grow an epitaxial Co₄N film, which shows four fold magnetic anisotropy in magneto-optic Kerr effect measurements. Detailed characterization using secondary ion mass spectroscopy indicates that N diffuses out when T_s is raised even to 400 K. Measurement of electronic structure using x-ray photoelectron spectroscopy and x-ray absorption spectroscopy further confirms it. Magnetization measurements using bulk magnetization and polarized neutron reflectivity show that the saturation magnetization of stoichiometric Co₄N film is even larger than pure Co. Since all our measurements indicated that N could be diffusing out, when Co₄N films are grown at high T_s , we did actual N self-diffusion measurements in a CoN sample and found that N self-diffusion was indeed substantially higher. The outcome of this work clearly shows that the Co₄N films grown prior to this work were always N deficient and the pathways for formation of a stoichiometric Co₄N have been achieved.

I. INTRODUCTION

Tetra transition metal nitrides of magnetic metals (M₄N; M = Fe, Co and Ni) are a class of compounds that have an anti-perovskite type fcc structure in which N atom resides at one-quarter of the octahedral interstices in an ordered manner. The insertion of N in the fcc metal lattice results in two inequivalent metal sites: one occupying the corner (M I) and others at face center (M II) positions of the cube as shown in fig. 1 (a). Here M II sites get hybridize with N atom but M I remain isolated from N. This results in localized magnetism at M I sites whereas itinerant magnetism at M II sites. The insertion of N causes an expansion in the lattice (compared to fcc host metal lattice)¹⁻⁶ and leads to very interesting magnetic properties such as higher saturation magnetization (Ms) due to a magneto volume effect.

The spin polarization ratio (SPR) of M₄N is higher than their host metals.^{2,7} Polarized electronic band structures of these M₄N compounds were calculated using the full-potential method.^{2,8} Among all M₄N, Co₄N is predicted to be the most effective material for spin-polarization of conducting electrons as its spin polarization ratios at the Fermi level reaches to about 90%.^{2,8} In addition, the insertion of N reduces the corrosion of metal and therefore M₄N compounds can be considered as a superior alternative to their pure metals in magnetic devices applications.^{7,9,10}

Larger Ms has been predicted theoretically for all M₄N compounds and observed experimentally for Fe₄N.

Whereas in case of Co₄N the value of Ms has always been found to be lower than the pure Co. In this connection, it may be noted that the theoretical value of lattice parameter (LP) for Co₄N is 3.735 \AA^1 but experimentally, it has been found anywhere between 3.59 to 3.52 \AA .¹¹⁻¹⁹ Since the LP of fcc Co is about 3.54 \AA ,¹ it appears that Co₄N thin films deposited so far might have mistaken for fcc Co. This can be envisaged by closely following the substrate temperature (T_s) used for deposition of Co₄N phase. We find that T_s between 435 to 725 K have been used and a correlation can be found between T_s and LP. Oda *et. al.* first attempted to prepare Co₄N films at $T_s = 435$ K and got LP = 3.59 \AA ,¹¹ at $T_s = 525$ K Silva *et. al.* found LP = 3.54 \AA .¹² When the T_s was even raised to 700 K and beyond, the LP remains at 3.54 \AA a value expected for fcc Co (not for Co₄N).^{13,14} It apparently looks that as T_s is raised N diffuses out from the system, leaving behind fcc Co as shown in fig. 1. Theoretically, it is expected that as N *at. %* decreases in Co₄N the LP should also decrease monotonically.^{1,20} Therefore, the LP of Co₄N can be used for estimating N deficiency in Co₄N. In our recent works we studied phase formations in Co-N system and found that at $T_s = 525$ K, fcc Co is formed, irrespective of the amount of N₂ gas used during reactive sputtering,²¹ however as the T_s goes down to 300 K, variety of Co-N phases emerge including Co₄N.²²

In absence of the phase diagram of Co-N system, it is difficult to assess the role of T_s on the phase formation of Co₄N thin films. Since the formation of Fe₄N thin films takes place typically at $T_s = 675$ K, similar high T_s have

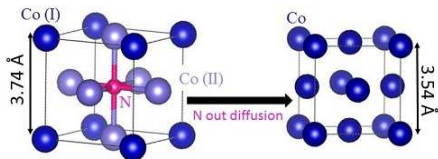


FIG. 1. (Color online) Schematic of conversion of Co_4N to fcc Co by N out diffusion.

been used for deposition of Co_4N films as well. The enthalpy of formation (ΔH_f°), is an important parameter that affects formation of any compound. For Fe_4N , $\Delta H_f^\circ \sim -12.17 \pm 20.72 \text{ kJ/mol}^{23}$ but for Co_4N it is significantly higher at about $0 \pm 2.896 \text{ kJ/mol}^3$. This may have consequences on the Co_4N phase formation that are addressed in this work.

First of all, we studied the effect of T_s on the phase formation of Co_4N thin films. In section III A, crystal structure, composition and morphology were studied and it was found that as T_s reduces the LP increases and its maximum value was found when $T_s = 300 \text{ K}$. Here, it can be anticipated that N diffuses out when T_s is raised. This assumption was further confirmed by measuring the electronic structure shown in section III B. Here both XPS and XAS measurements confirm that sample becomes highly N deficient even at $T_s = 400 \text{ K}$. Magnetization measurements presented in section III C clearly show a loss in saturation magnetization with LP in agreement with theoretical predications for Co_4N . In section III D, we show that by reducing the target size, the formation of Co_4N takes place from the ‘metallic state’ of target and then fully stoichiometric Co_4N phase can be realized. Under optimized conditions, epitaxial Co_4N was grown and it exhibits a four fold magnetic anisotropy expected for cubic symmetry as discussed in section III E. From all these measurements, it becomes obvious that N diffusion should be much larger in the Co-N system as compared to similar systems (e.g. Fe-N). Since N self-diffusion in Co-N was not measured before, we measured N self-diffusion in CoN and compared it to FeN as shown in section III F. Overall, the results presented here aims to find the pathways for a stoichiometric Co_4N . After achieving this, detailed analysis of structural, electronic and magnetic properties is presented and discussed in this work.

II. EXPERIMENT

A series of Co-N thin films were prepared on different substrates (SiO_2 , Si and LaAlO_3 (100)) using direct current magnetron sputtering (dcMS) system (Orion-8, AJA Int. Inc.). Co target (99.95%) ($\phi = 3 \text{ inch}$) were sputtered using a mixture of argon (99.9995%) and nitrogen (99.9995%) gases flowing through two different mass flow controllers. The partial gas flow of nitrogen (R_{N_2}

$= p_{\text{N}_2}/(p_{\text{Ar}} + p_{\text{N}_2})$, where p_{Ar} and p_{N_2} are gas flow of Ar and N_2 gases, respectively) was kept at 20%, a value favoring in growth of Co_4N phase.^{21,22,24} A base pressure of $2 \times 10^{-7} \text{ Torr}$ was achieved before deposition and the working pressure was maintained at 3 mTorr during deposition. Keeping all other parameters constant, substrate temperature (T_s) was kept at 300 (no intentional heating), 325, 350, 375 and 400 K. The thicknesses of the films were ranging from 1200 to 1400 Å. In addition, another set of Co-N thin films were also grown by $\phi = 1 \text{ inch}$ Co target (99.95% purity) at different values of $R_{\text{N}_2} = 0, 5, 10, 12, 20, 25, 30, 40$ and 100% where T_s was kept at 300 K (all other deposition parameter were kept same as above mentioned).

Deposited samples were characterized for their long range ordering and phase formation by x-ray diffraction (XRD) using a standard x-ray diffractometer (Bruker D8 Advance) having $\text{CuK}\alpha$ x-ray source. To get the information about the atomic concentration of nitrogen in deposited samples, secondary ion mass spectroscopy (SIMS) depth profiling measurements were carried out using a Hidden Analytical SIMS workstation. A primary O_2^+ ions source was used for sputtering with an energy of 4 keV and beam current of 200 nA. SIMS measurements were performed in a UHV chamber with a base pressure of the order of $5 \times 10^{-10} \text{ Torr}$ while during measurements the chamber pressure was $1 \times 10^{-7} \text{ Torr}$. The sputtered secondary ions were detected using a quadrupole mass analyzer. Morphology of the deposited samples were studied by atomic force microscopy (AFM) in non contact mode. Electrical resistivity was measured in a four probe mode at room temperature. X-ray photoelectron spectroscopy (XPS) measurements were carried out using Al-K α lab source. Prior to XPS measurement, samples were sputtered with an ion energy of 1 kV and current of 4 μA . To investigate the local and electronic structure, x-ray absorption near edge spectroscopy (XANES) was performed in the total electron yield (TEY) mode at BL-01²⁵ at the Indus-2 synchrotron radiation source at RRCAT, Indore. The XANES measurements were carried out in a UHV chamber with a base pressure of $2 \times 10^{-10} \text{ Torr}$. To avoid surface contaminations, samples were cleaned *in-situ* using a Ar^+ source with an energy of 5 keV kept incident at an angle of 45°. The magnetization measurements were carried out at room temperature using a Quantum Design SQUID-VSM (S-VSM) magnetometer. Polarized neutron reflectivity (PNR) measurements were performed at AMOR beamline, SINQ, PSI Switzerland in time of flight mode. During PNR measurements, to saturate the sample magnetically, a magnetic field of 0.5 T was applied parallel to the sample’s surface. Reciprocal space mapping (RSM) and Phi scans were performed with high resolution x-ray diffractometer (Bruker D8 Discover). Magnetic anisotropy was studied in longitudinal mode using magneto optical-Kerr effect (MOKE) and Kerr microscopy (Evico Magnetics) equipment.

III. RESULTS AND DISCUSSION

A. Structure, morphology and composition of Co_4N films

Fig. 2 shows the XRD patterns of Co-N thin films deposited at $T_s = 300, 325, 350, 375$ and 400 K. For reference, XRD pattern of a Co thin film of similar thickness is also included here. In the Co thin film, we can observe peaks at 41.9 and 47.5° corresponding to (100) and (101) planes, respectively for hcp structure (JCPDS 050727).²⁶ In addition, the peak at 44.7° coincides with (111) plane of fcc and (002) plane hcp Co. Generally, Co stabilizes in the hcp structure under ambient conditions and show an allotropic transition from hcp to fcc at high temperature (above 690 K). But, the occurrence of hcp and fcc biphas usually takes place in thin films and nanoparticles.^{26,27}

The XRD patterns of samples prepared using partial nitrogen gas flow, show prominent peaks around $43, 50$ and 74° and they can be respectively assigned to (111), (200) and (220) planes of fcc Co_4N structure.¹¹ We can clearly see as the T_s is raised, peaks gradually shift towards higher 2θ values. This immediately indicates that the LP (obtained from (200) peak) is decreasing with an increase in T_s as shown in the inset (a) of fig. 2. Such lowering of LP may be due to N deficiency in Co_4N . In recent theoretical studies, it was shown that the LP is directly correlated with the N *at.*% in Co_4N . It was found that as the amount of N decreases (considering a supercell of 8 unit cells of Co_4N) the LP also reduces^{1,20} as shown in fig. 3 and therefore LP may be used to estimate N concentration in Co_4N . Table. I compares values of LP and N *at.*% measured experimentally using the formalism of Mater *et. al.*¹ From here, it is clear that N *at.*% and LPs get reduced as T_s increased, which elucidate that a compression in the Co_4N lattice takes place probably due to N out diffusion from the lattice at higher T_s .

As we find that the LP increases by decreasing T_s , at the lowest $T_s = 300$ K, obtained value of $LP = 3.65 \text{ \AA}$. This values is about 3% smaller than the theoretical value (3.735 \AA). To further enhance it, we have addressed the issues related with target poisoning in reactive sputtering and they are discussed in detail in section III D. We find that when the Co_4N phase emerges out of the metallic state of the target, LP can be enhanced further to 3.7 \AA . This is the highest value of LP of Co_4N found so far as shown by an asterisk (*) in the inset (a) of fig. 2.

In addition, we found that the XRD peak shape of Co-N samples shows an asymmetry, especially for those with $T_s \leq 350$ K. This asymmetry is marked by an arrow (\downarrow) for $T_s = 300$ K sample and can be fitted if we consider (101) reflection of hcp $\text{Co}_3\text{N}_{1-x}$. It indicates that Co_4N formed with small amount of $\text{Co}_3\text{N}_{1-x}$ phase. At higher T_s (≥ 350 K) this asymmetry disappears indicating that hcp phase transforms into fcc.

Our XRD measurements show that the Co_4N becomes N deficient as T_s is raised. This can also be seen among various works on Co_4N available in the literature. For

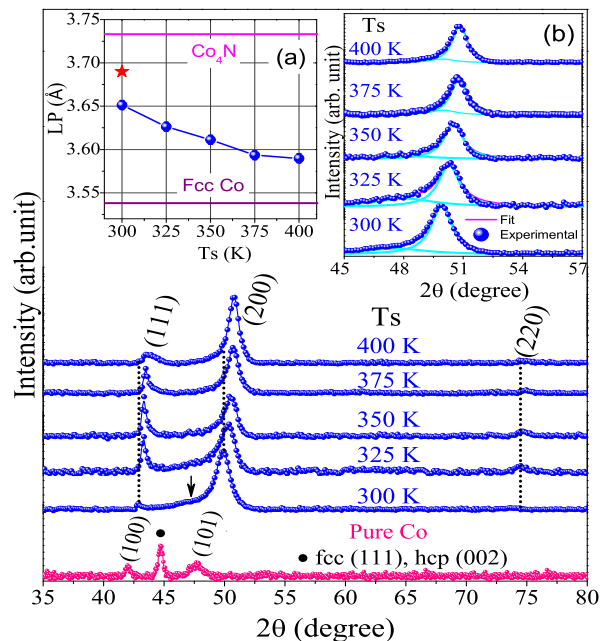


FIG. 2. (Color online) XRD patterns of Co-N thin films deposited at different T_s from 300 to 400 K. Inset showing the variation of LP with respect to T_s (a) and fitted XRD curves along (200) reflection (b). The error bars in estimation of LP are typically the size of symbols used here.

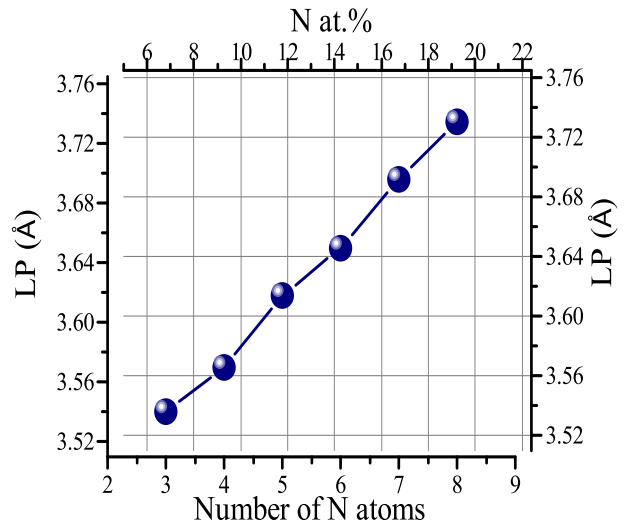


FIG. 3. (Color online) Theoretical correlation of LP with N *at.*% and no. of N atom in a supercell (having 8 unit cell) of Co_4N lattice.

TABLE I. Relationship between LP and N *at.*% for Co_4N determined experimentally from XRD and SIMS measurements.

T_s (K)	LP (\AA)	N (XRD) (<i>at.</i> %)	N (SIMS) (<i>at.</i> %)
300	3.65	15	15 ± 2
325	3.63	13	-
350	3.61	12	12 ± 2
375	3.59	12	-
400	3.58	10	7 ± 2

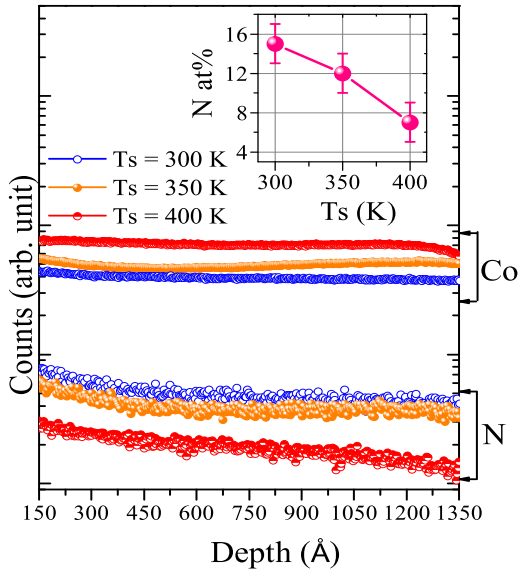


FIG. 4. (Color online) SIMS depth profiles of Co-N thin films deposited at $T_s = 300, 350$ and 400 K. Inset shows the variation of N $at.\%$ as a function of T_s .

$T_s = 440$ K, Oda *et. al.* found $LP = 3.586 \text{ \AA}$,¹¹ Silva *et. al.* and Wang *et. al.* found the $LP = 3.54$ and 3.56 \AA for $T_s = 525$ K,^{12,16} at $T_s = 625$ and 725 K, K. Ito. *et. al.* found $LP = 3.52 \text{ \AA}$.^{13,14} From here it appears that a stoichiometric Co_4N phase has not been formed before as in all works higher T_s was used. As we find that at higher T_s even Co appears in the fcc phase and its LP at 3.54 \AA is only about 5% lower than that Co_4N , therefore fcc Co has been mistaken for Co_4N phase. To further confirm this, we measured N $at.\%$ in our samples using SIMS.

SIMS depth profiles of Co and N for samples deposited at $T_s = 300, 350$ and 400 K are shown in fig. 4. We can see that as T_s is increasing, N signal goes down while that of Co goes up. This gives a direct evidence that N is diffusing out of Co_4N even when T_s is just raised to 350 K. We can see that our Co profiles are almost constant throughout the depth of sample but N profiles are somewhat skewed near surface regions. This may also indicate that N is diffusing out from the surface as one would expect, but large depth resolution of SIMS (~ 50 - 100 \AA) and poor signal does not allow to quantify N out diffusion. However, by sandwiching a thin $Co^{15}N$ marker layer between $Co^{nat}N$ layers, we measured N self-diffusion and results are presented in section III F.

Still N depth profiles can be used to estimate the N concentration. Using a reference samples and following a procedure described in earlier works,^{21,22,24} we obtained N $at.\%$, as shown in the inset of fig. 4. Since N profiles are somewhat skewed, an average value was taken in the middle of the layer in all samples. We can clearly see that N $at.\%$ is decreasing almost linearly with T_s , in agreement with XRD results presented in table. I.

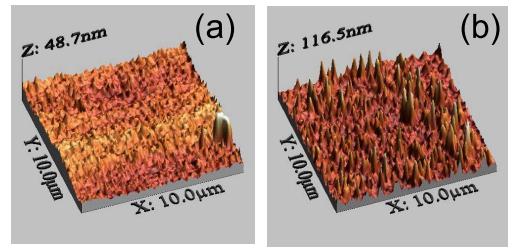


FIG. 5. (Color online) 3D view of AFM images of Co-N thin films deposited at $T_s = 300$ K (a) and 400 K (b).

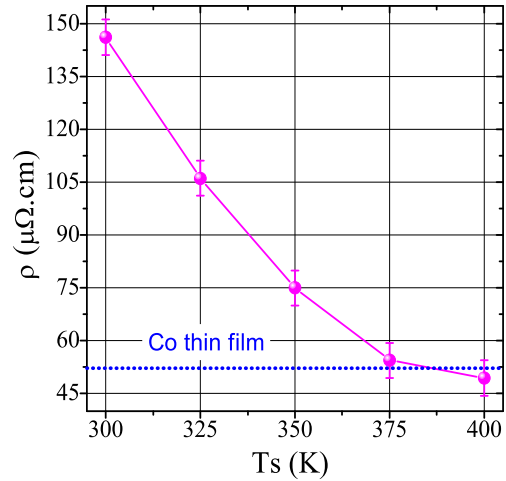


FIG. 6. (Color online) Dependence of electrical resistivity (ρ) of Co-N thin films on T_s .

As N out diffusion takes place it may also affect the microstructure. We can see from our AFM images (fig. 5) that the surface morphology of sample deposited at $T_s = 300$ K is smoother than the one deposited at 400 K. It appears that N out diffusion leaves behind a spike like microstructure leading to larger surface roughness.

We also measured the electrical resistivity (ρ) in our samples and as can be seen in fig. 6, it decreases as T_s increases. In earlier studies performed in the Co-N system, it was demonstrated that ρ maximizes with N $at.\%$.^{18,19,28} Since in our samples N $at.\%$ is maximum for $T_s = 300$ K sample, the value of ρ is also maximum and it decreases almost linearly as N $at.\%$ decreases by increasing T_s . It may be noted that for $T_s = 400$ K sample the value of ρ becomes comparable to a pure Co thin film. In agreement with other results, our electrical resistivity also confirm that N is diffusing out when T_s is raised during deposition of Co_4N thin films.

B. Electronic Structure

We did XPS and XAS measurements to study the electronic structure of our samples. Fig. 7(a) and (b) shows N 1s and Co $2p_{3/2}$ spectra for samples deposited at $T_s =$

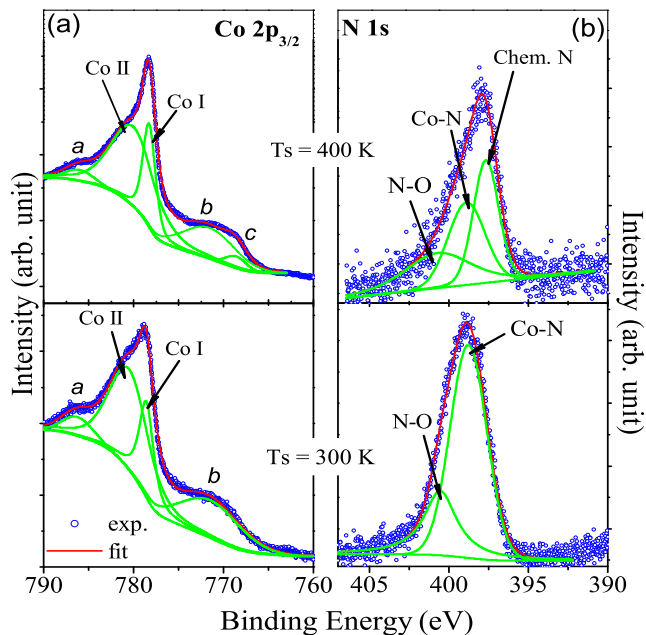


FIG. 7. (Color online) Co 2p_{3/2} (a) and N 1s (b) XPS spectra of Co-N thin films deposited at T_s = 300 and 400 K.

300 and 400 K and they were fitted using XPS peak fitting software. N 1s and Co 2p_{3/2} spectra are significantly different for both samples. In N 1s spectra, features corresponding to N-O (400.5 eV) and Co-N (398.6 eV) can be seen in both samples. Presence of N-O feature can be understood due to some surface oxidation (through measurements were done after surface cleaning by sputtering) and the Co-N feature stems from the bonding between Co and N. We find that the area of the Co-N feature is about 4 times larger in T_s = 300 K sample. On the other hand, a prominent feature for chemisorbed N₂ (chem. N = 397.5 eV) can only be seen in T_s = 400 K sample. Weak Co-N and the presence of chem. N features clearly signifies that some nitrogen has diffused out and accumulated near surface regions (in agreement with SIMS data shown in fig. 4). Such signature of chem. N has also been seen in Fe₄N thin films after annealing in presence of N₂ gas.²⁹ and also in other studies when N diffuses out from metal nitrides.^{29–31}

In order to fit the Co 2p_{3/2} spectra, structural aspect of Co₄N should also be considered. As shown in fig. 1, Co sites (I and II) are different where Co II only has direct bonding with N. We find that our Co 2p_{3/2} can be fitted mainly with these Co I and Co II components occurring at 778.5 and 780.5 eV, respectively. We find that the fraction of Co I (Co II) increases (decreases) when T_s is raised to 400 K. This is in agreement with N 1s spectra and can happen when the fraction of Co atoms un-bonded with N increases. In addition, some features assigned as ‘a’, ‘b’ and ‘c’ can also be seen. Here ‘a’ may be due to shake-up transition³² which is usually observed in the metals while features ‘b’ and ‘c’ are due to the L₃VV Auger transition.³³

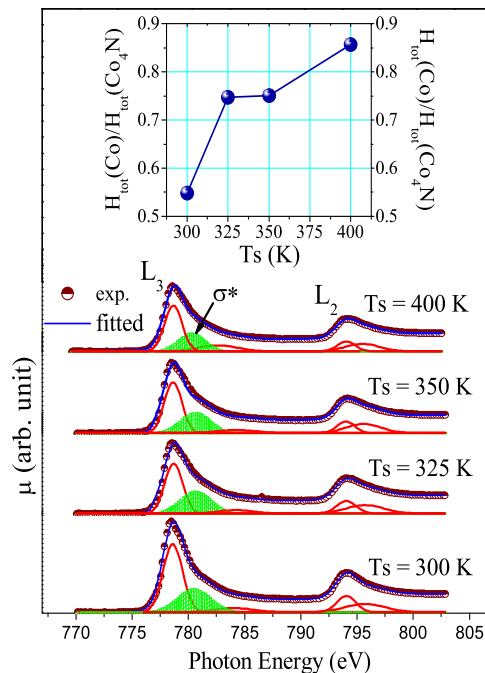


FIG. 8. (Color online) Co L edge XANES spectrum of Co-N samples deposited at T_s = 300, 325, 350 and 400 K. Inset shows the variation in H_{tot}(Co)/H_{tot}(Co₄N) with T_s, here error bars are typically the size of symbols.

Fig. 8 show the Co L-edge XAS spectra of Co₄N thin films deposited at T_s = 300, 325, 350 and 400 K. Two main spectral features were observed around 778 eV (L₃) and 794 eV (L₂). They arise due to well-known spin-orbit splitting of the Co 2p core-hole (2p⁶3dⁿ → 2p⁵3dⁿ⁺¹) transition. We used Athena software³⁴ to fit XAS spectra using a step and Gaussian function after pre and post-edge normalization. Co L₃ edge can be deconvoluted into three (~ 778, 780, 784 eV) and L₂ into two (794 and 795 eV) sub spectra. Here the peaks at ~778 and 784 eV correspond to the Co I site in Co₄N. On the other hand, the peak at ~780 eV (shown as shaded region in fig. 8) corresponds to σ* anti-bonding which occurs due to a strong hybridization of ‘pd’ states between Co II and N atoms in Co₄N.^{35,36} We can clearly see that the σ* feature becomes weak as T_s is increasing indicating reduced hybridization between Co and N. From the fitting of this peak, hybridization between Co and N can be quantified. Compared to T_s = 300 K sample, it reduces by about 13, 21 and 38% as T_s is raised to 325, 350 and 400 K, respectively.

In agreement with other results, XAS measurements also confirm that the fraction of Co atoms un-bonded with N increases as T_s is increased. This can be further confirmed by directly comparing the overall intensities of L-edges. It is known that the sum of amplitudes of L₃ and L₂ edges in XAS is proportional to number of holes (H_{tot} = HL₃ + HL₂, where HL₃, HL₂ is the amplitude of L₃ and L₂ edges) present in d state of the metal.^{37,38} Comparing H_{tot}(Co₄N) for Co-N samples together with

$H_{\text{tot}}(\text{Co})$ for a pure Co film can yield variances between them as for $N \rightarrow 0$, $\frac{H_{\text{tot}}(\text{Co})}{H_{\text{tot}}(\text{Co}_4\text{N})} \rightarrow 1$. As shown in the inset of fig. 8, $H_{\text{tot}}(\text{Co})/H_{\text{tot}}(\text{Co}_4\text{N})$ increases from 0.55 to about 0.85 when the T_s is raised from 300 to 400 K. Since later is approaching to unity confirming that the amount of N is becoming negligible due to N out-diffusion.

Both XPS and XAS measurements unambiguously confirm the phase formation of Co_4N at $T_s = 300$ K and when it is raised to 400 K, substantial amount of N diffuses out leaving behind mainly fcc Co.

C. Magnetic properties

To measure the saturation magnetization (M) in our samples, bulk magnetization (SQUID-VSM) and PNR measurements were carried out. It may be noted that mostly bulk magnetization measurements have been used to deduce M in Co_4N thin films. Due to ambiguities in estimating sample volume and density, there may be errors in estimating correct M , which is evident from large variations observed (between 46 to 150 emu/gm and 485 - 1300 emu/cc) in Co_4N thin films.^{11-13,15-17,39} On the other hand since in PNR, the sample volume and substrate demagnetization effects do not play a role in measurement of M , we did PNR for precise measurement of M in our samples. Fig. 9 shows PNR and M-H loops of samples deposited at different T_s . The inset (a) of fig. 9 shows M-H loops and the inset (b) compares the coercivity (H_c). We find that H_c is small indicating that samples are soft magnetic and it almost decreases linearly as T_s increases.

From the M-H loops, we find that $M = 1304, 1286, 1262$ and $1174(\pm 20)$ emu/cc for $T_s = 300, 325, 350$ and 400 K, respectively. PNR patterns of our samples are shown in fig. 9. From the fitting of these (using GenX⁴⁰), we find that $M = 1.73 \pm 0.05 \mu_B/\text{Co}$ atom for $T_s = 300$ K sample while for $T_s = 325, 350$ and 400 K samples it comes out to be about $1.65 \pm 0.05 \mu_B/\text{Co}$ atom. Clearly both S-VSM and PNR measurements suggest that the value of M is the largest for $T_s = 300$ K sample and decreasing as T_s is increasing. This behavior can be understood from the well-known high-volume high-moment derived for tetra metal nitrides.^{1,2} An empirical relation for a binary alloy (consisting of elements A and B) between LP and M is given by:⁴¹

$$LP = a_A(1-x) + a_Bx + CM \quad (1)$$

Where, a_A, a_B and C are the constant like parameters and x is the atomic fraction. However, the exact quantification of M is not possible using eq. 1 due to ambiguities in exact calculation of constants.⁴¹ Alternatively, using a rather simplistic approach based on the atomic theory model and considering the dependence of LP on the composition of Co_4N as shown in fig. 3, we can calculate M for samples deposited at different T_s .

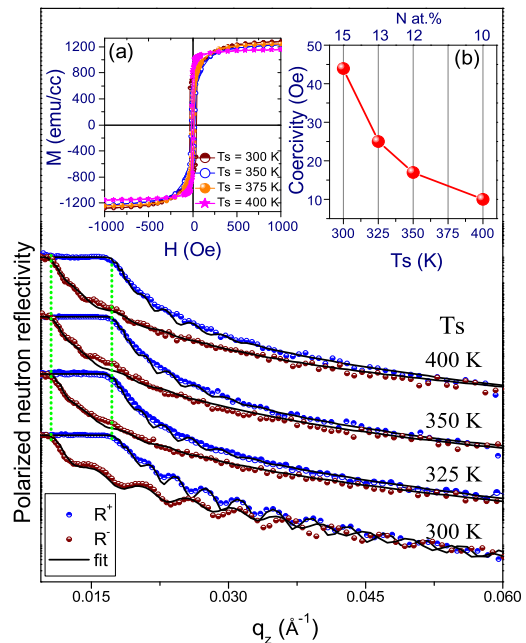


FIG. 9. (Color online) Fitted PNR spectra of Co-N thin films deposited at $T_s = 300, 325, 350$ and 400 K. Inset showing the M-H hysteresis loop (a) and variation of coercivity of these samples as a function of T_s (b). Typical errors in the value of coercivity is the size of symbol used here.

TABLE II. Magnetic configuration of Co I and Co II sites in Co_4N .

Co site	Coordinate	d occupancy	μ	nu	nd
I	(0,0,0)	$3d^8$	2	0	1
II	(0,1/2,1/2)	$3d^7$	3	1	0
II	(1/2,0,1/2)	$3d^7$	3	1	0
II	(1/2,1/2,0)	$3d^7$	3	1	0

By considering the postulates of atomic theory that (i) filling of electrons according to Hund's rule (ii) overlapping of nearest neighbor will cause antiparallel alignment of 3d shell. In the Co_4N structure Co I and Co II sites (as shown in fig. 1) contribute in determination of M as:^{42,43}

$$M = (nu_{II} - nd_{II})\mu_{II} + (nu_I - nd_I)\mu_I \quad (2)$$

Here, nu_{II} and nd_{II} are number of Co II sites having spin up and down electrons, respectively. Similarly nu_I and nd_I can be interpreted for Co I. μ_I and μ_{II} is the resultant moment of Co I and Co II, respectively. Magnetic configuration of these sites is given in table II. Using eq. 2 and table II, we get $M = (3-0)3 + (0-1)2 = 7 \mu_B$ per f.u., yielding $M = 1.75 \mu_B/\text{Co}$ atom for stoichiometric Co_4N . This is in agreement with theoretical calculations based on DFT calculations.^{1,3} Considering a similar approach described in section III A, in a supercell having 8 unit cells of Co_4N and by sequentially taking out one N atom, we get $M = 1.74, 1.73$ and $1.72 \mu_B/\text{Co}$ atom for LP = 3.65, 3.63 and 3.57 Å corresponding to N at.% = 15, 13

and 10%, respectively. Broadly these theoretical calculations are in agreement with our experimental results.

D. Target poisoning affecting Co_4N phase formation

From the above results, we have shown that Co_4N thin film attains the highest value of LP as T_s is lowered and N *at.*% also increases. We find that LP was maximum for $T_s = 300\text{ K}$ sample at $3.65(5)\text{ \AA}$ and the amount of N in Co_4N was $15\pm 2\%$. Both these are somewhat smaller than the theoretical values: for stoichiometric Co_4N , LP should be 3.735 \AA and N concentration at $20\text{ at.}\%$.¹ Since further lowering of T_s may produce a disordered phase, other parameters that could influence stoichiometry of Co_4N film were considered.

In a reactive sputtering process, variations in the deposition rate (D_R) with the amount of reactive gas is a key for phase formations. When the D_R is similar to elemental metal target, it is referred as ‘metallic state’ and when D_R become very small (compared to metallic state), target is in ‘poisoned state’ due to compound formation taking place at the target itself. In between these two states is a ‘transient state’ which is rather ill-defined. When a compound is formed from such ‘transient state’, it is affected by so called hysteresis effects.^{44–50} We measured D_R by depositing a series of Co-N thin films at $T_s = 300\text{ K}$ by systematically increasing R_{N_2} during deposition. Thicknesses were measured using x-ray reflectivity and obtained D_R are shown in fig. 10 (a). We find that for $R_{\text{N}_2} = 0\text{--}10\%$, the target is in ‘metallic state’ (region I), between $15\text{--}50\%$ it is in ‘transient state’ (region II) and above this R_{N_2} values, it attains the ‘poisoned state’ (region III). Since the Co_4N phase was formed for $R_{\text{N}_2} = 20\%$, it emerges from the ‘transient state’ of the target and therefore even a slight variation in R_{N_2} could vary the composition.

A lot of efforts have been made to produce hysteresis free films in reactive sputtering process. Some of efforts realize on enhancing the ionic concentration by doing high power impulse magnetron sputtering.⁴⁷ A novel approach within the dc magnetron sputtering process was shown for aluminium oxides by reducing the target erosion area. This essentially reduces the consumption of reactive gas in target poisoning and extending the ‘metallic state’ of the target.⁴⁶ These effects were also demonstrated in theoretical models proposed by Berg et al.^{44,45}

Since in our case when we use a 3 inch diameter Co target, the Co_4N phase was forming from the ‘transient state’ and it was under stoichiometric, we attempted to prepare the Co_4N phase from a smaller 1 inch diameter Co target at $T_s = 300\text{ K}$. As can be seen from fig. 10 (b), the ‘metallic state’ has now been extended and the ‘transient state’ has narrowed down but the ‘poisoned state’ has also been extended. This implies that the smaller target remains rather insensitive to the reactive gas flow in the beginning but it becomes even more sensitive (than larger target) to the reactive gas at higher flows

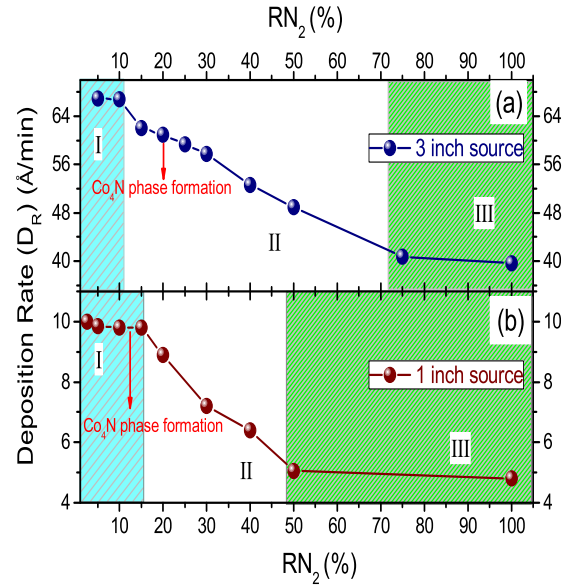


FIG. 10. (Color online) Variation of deposition rate with R_{N_2} in Co-N thin films deposited using 3 (a) and 1 inch (b) targets. Here region ‘I’ corresponds to the ‘metallic state’ of target, region ‘II’ denotes to the ‘transition’ and ‘III’ to the ‘poisoned state’ of Co target. Errors in deposition rates are lower than the size of symbols used here.

of reactive gas. This may happen as ion implantation of reactive gas becomes more dominant in the smaller area source. This behavior is in agreement with modified Berg’s model.⁴⁴

From the 1 inch Co target, we find that Co_4N phase is forming already at $R_{\text{N}_2} = 12\%$ (within the ‘metallic state’) as shown in fig. 11 (b). A comparison of this sample together with Co_4N sample deposited with 3 inch source clearly shows that the (200) XRD peak is shifted to lower angle and the obtained value of LP is $3.69(5)\text{ \AA}$ which is very close to its theoretical value and is the highest value obtained so far for Co_4N thin films. Our SIMS measurements (not shown here) also confirmed that N concentration is about $18\pm 2\%$. Clearly by reducing the target area, optimizing T_s we could deposit the stoichiometric Co_4N phase matching well with its theoretical values. However, it may be noted that overall deposition rates decrease significantly when the smaller source was used.

Magnetization of this sample was also measured and PNR and MH curves are compared for Co_4N thin films deposited using 1 and 3 inch sources as shown in fig. 11 (b, c). From PNR we can see that the R^+ is slightly shifted to higher q_z values in Co_4N thin film deposited using 1 inch source indicating that M is higher here, although it is not as noticeable from the M-H loop. From the fitting of PNR data we obtained $M = 1.75\mu_B/\text{Co}$ atom which is slightly higher than the Co_4N sample deposited with the 3 inch Co source. These results are can be understood due to a small rise in LP of Co_4N film when deposited

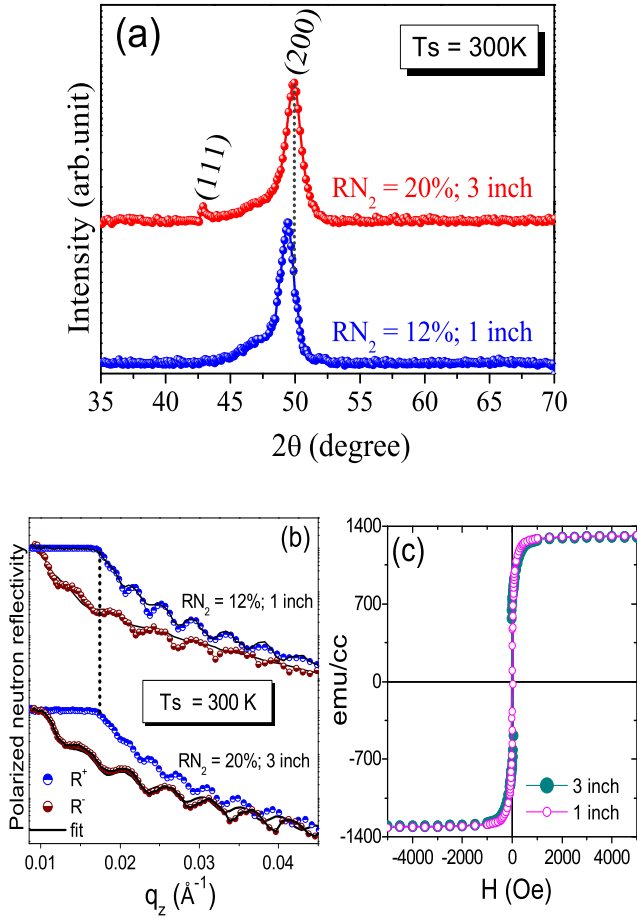


FIG. 11. (Color online) XRD patterns Co-N thin films deposited at $R_{N_2} = 12$ and 20% using 1 and 3 inch Co targets, respectively both at $T_s = 300\text{ K}$ (a), fitted PNR patterns (b) and M-H hysteresis curves of these thin films (c).

with the 1 inch Co source.

E. Epitaxial Co_4N film

So far, we have discussed about finding pathways for a stoichiometric Co_4N film and got its LP up to about 99% of the theoretical value. This was achieved by depositing samples at $T_s = 300\text{ K}$ and using the ‘metallic state’ in a 1 inch Co target during the reactive sputtering process. These optimized conditions were applied to deposit a Co_4N thin film on a LaAlO_3 (LAO) substrate oriented along (100) plane. Since LAO has a very small lattice mismatching with Co_4N ($\sim 1.3\%$), it is most suitable to grow an epitaxial Co_4N thin film. As a reference, a polycrystalline sample was again deposited on a quartz (SiO_2) substrate together with that on LAO. Fig. 12 (a) shows XRD pattern of Co_4N film deposited on LAO and quartz substrate and for comparison XRD pattern taken on the bare LAO substrate is also shown. In agreement with fig. 11(a), the Co_4N sample on the quartz substrate

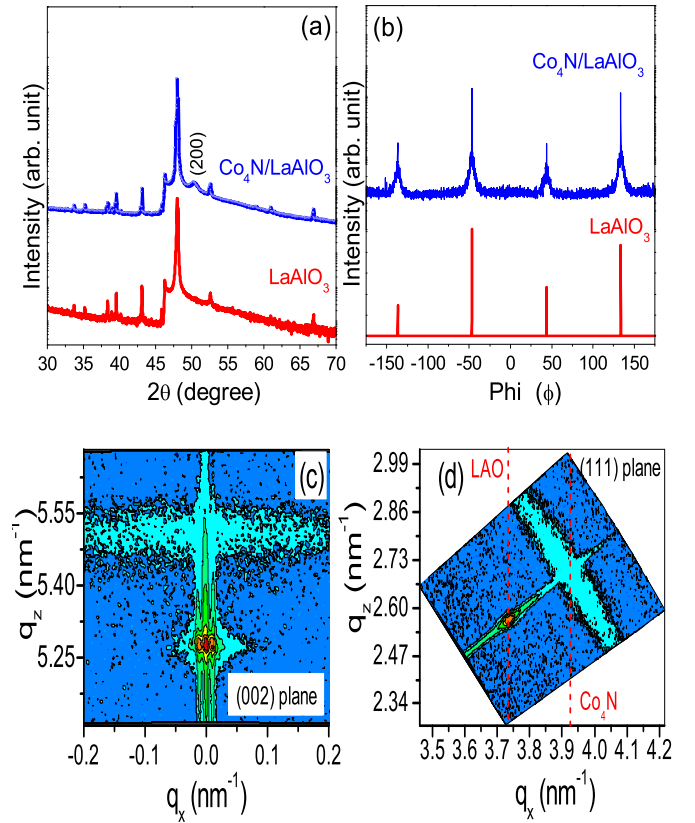


FIG. 12. (Color online) XRD spectra (a) and Phi scan along (100) plane (b) of Co_4N thin film grown on LAO (100) substrate. Reciprocal space mapping of Co_4N thin film deposited at LAO (100) substrate (c).

is identical but on the LAO substrate has (200) plane at a slightly higher angle. The LP for the Co_4N film on LAO substrate comes out to be 3.635 \AA .

To confirm the epitaxial nature of the sample deposited on LAO substrate, Phi scan along (100) plane (fig. 12 (b)) and RSM measurements were carried out. Here the Phi scan of substrate shows a very clear four fold reflections which occur in cubic symmetry. Similarly, the reflections from film are also completely overlapping the substrate peaks, conforming the epitaxial growth of Co_4N thin film on LAO substrate.

Fig. 12 (c) and (d) shows RSM scans for this sample along (002) and (111) planes, respectively. From here we deduced out-of-plane (002) and in-plane (111) LP that comes out to be 3.635 \AA and 3.71 \AA , respectively. Since the film on the quartz substrate was found to be fully stoichiometric Co_4N having LP $\sim 3.7\text{ \AA}$, the film on the LAO substrate is also expected to be stoichiometric. The discrepancy in LP for Co_4N film deposited on LAO substrate may arise if it has a tensile strain along in-plane and a compressive strain along the out-of-plane direction. If this strain stems from a lattice mismatch between film and substrate, the broken lines shown in fig. 12 (d) should have appeared at similar q_x values.^{51,52} But since they

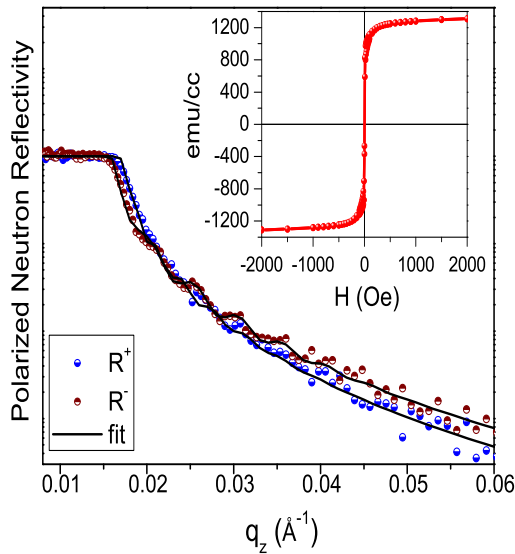


FIG. 13. (Color online) Fitted PNR spectra of epitaxial Co_4N thin film on LAO substrate. Inset showing the M-H hysteresis loop of the same sample.

are well-separated, the strain could be within the film itself leading to different values of in-plane and out-of-plane LP. In addition, it may be noted that the spot corresponding to Co_4N film in fig. 12 (d) is quite broad and also the width of Phi reflections in fig. 12 (b) is large. Both these indicate a mosaic type epitaxial growth.^{51,52} This could be due to the fact that at low T_s (300K) adatoms would not have sufficient energy to establish the long range ordering to its fullest.

The PNR and M-H loop for the epitaxially grown Co_4N thin film are shown in fig. 13. Since the scattering length density of LAO substrate is large, the splitting between R^+ and R^- is not as appreciable as found for the polycrystalline sample deposited on quartz (SiO_2) substrate. From the M-H loop M comes out to be ~ 1320 emu/cc and from PNR measurements, it is $\sim 1.75\mu_B/\text{Co}$ atom. Both these values are matching well with polycrystalline Co_4N sample deposited under similar conditions.

The influence of epitaxy on the magnetic property was investigated from MOKE and Kerr microscopy measurements e.g. the presence of cubic symmetry should appear in the polar plot of squareness ($S = M_r/M_s$; here M_r and M_s are remanence and saturation magnetization) with the applied field angles. This has been amply demonstrated for Fe_4N thin films but not yet for Co_4N .⁵³ We measured hysteresis loops (in longitudinal MOKE setup) by changing the angle of applied magnetic field at an interval 10° between 0 and 180° assuming similar for other two quadrants. They are shown in fig. 14 (A) for representative angles of 0, 20, 40 and 90° . Further, we can clearly see presence of two loops and to quantify them, they were fitted using:^{54,55}

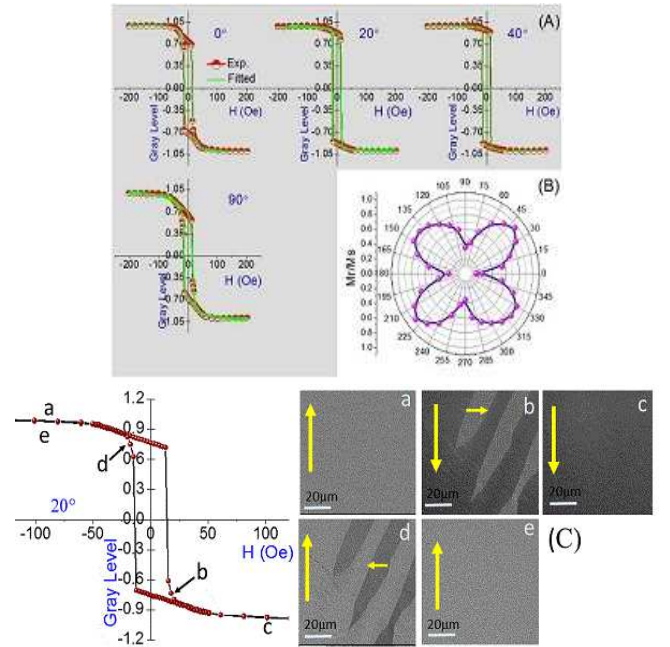


FIG. 14. (Color online) Longitudinal MOKE hysteresis loops of epitaxial Co_4N thin film (A). Polar plot of squareness (M_r/M_s) and coercivity with applied field angle (B). Kerr domain evolution images of epitaxial Co_4N thin film for 20° hysteresis loop (C).

$$M(H) = \sum_i \frac{2Ms^i}{\pi} \left[\left(\frac{H \pm Hc^i}{Hc^i} \right) \tan\left(\frac{\pi S^i}{2}\right) \right] \quad (3)$$

From the fitting, we obtain two magnetic contributions having coercivity, $H_c \sim 15$ and 40 Oe and their corresponding amount comes out to be about 94 and 6%, respectively. Here, it appears that majority fraction should be due to Co_4N phase and the minor one could be due to some Co impurity. In addition, the fitting of these loops yields variation of the S as a function of applied field angles shown in the polar plot fig. 14 (B). The polar plot clearly shows an in-plane biaxial magnetic anisotropy (four fold). As expected, we can see that easy and hard magnetization axes are along (100) and (110) direction, respectively. Such four fold anisotropy is expected due to cubic symmetry and confirm the epitaxial growth of Co_4N as evidenced earlier for epitaxial Fe_4N thin films.⁵³ In agreement with XRD measurements, our MOKE measurements also confirm the epitaxial nature of Co_4N thin films deposited on LAO substrate. Here the magnetocrystalline constant (K) can be estimated assuming that the anisotropy field is nearly equal to the saturation field and comes out to be $\sim 1.2 \times 10^4 \text{ J/m}^3$ which is smaller than that of Co ($\sim 10^5 \text{ J/m}^3$) but close to Fe_4N .⁵³ Furthermore, a reversal process by 90° domain wall nucleation should take place when the magnetic field is applied in between easy and hard axes.⁵³ This can be evidenced in Kerr microscopy images as shown in fig. 14(C). Images were captured at points a(=e), b, c, and d and

shown there for an applied field angle of 20° . The 180° magnetization reversal can be clearly seen from the image *a* to *e* followed by two consecutive 90° domain wall nucleation in image *b* and *d* (shown by arrow).

F. N Self Diffusion in Co-N

The results obtained from this work can be understood if N is diffusing out from Co-N even if we raise the T_s above 300 K. Signatures of such N out-diffusion can be clearly seen in the N depth profiles shown in fig. 4. However, to quantify it, N self-diffusion should be measured. We find that N self-diffusion in the Co-N system has not been measured before. Following a similar approach adopted for the FeN thin films,^{56–58} we prepared a sample $\text{Co}^{\text{nat}}\text{N}(100\text{ nm})|\text{Co}^{15}\text{N}(2\text{ nm})|\text{Co}^{\text{nat}}\text{N}(100\text{ nm})$ on a Si substrate at $T_s = 300\text{ K}$ and under identical conditions that were used to prepare the FeN sample.^{56,57} For determining the diffusivity of N, SIMS depth profiles were measured after isochronal thermal annealing at different temperatures for 1 hour at each temperature and are shown in fig. 15. Due to thermal annealing, ^{15}N profiles get broadened and the width of this peak has been used to deduce the diffusivity:^{56,57}

$$D(t) = \frac{\sigma_t^2 - \sigma_o^2}{2t} \quad (4)$$

Where, $D(t)$ is the time-averaged diffusion coefficient and σ_t is the standard deviation (before annealing; $t = 0$ and after an annealing time t) obtained after fitting ^{15}N profiles to a Gaussian function as shown in fig. 15. Using eq. 4, diffusivity (D) of N has been measured at different temperatures and follows an Arrhenius type behavior given by:

$$D = D_o \exp(-E/k_B T). \quad (5)$$

Here, D_o denotes the pre-exponential factor, E the activation energy, T annealing temperature, and k_B is the Boltzmanns constant. Using eq. 5 we get a straight line as shown in inset of fig. 15, yielding activation energy $E = 0.5 \pm 0.05\text{ eV}$. Here it may be noted that this activation energy is valid only for the isochronal annealing treatment and relaxation of diffusivity was not taken into account. We can now directly compare the diffusivity of N in FeN together with that in CoN. In FeN we find that ^{15}N profile can still be seen when the sample was annealed at 600 K ⁵⁶ whereas, it completely disappears above 500 K as shown in fig. 15. Also the activation energy for N self-diffusion in FeN is typically about 1.5 eV .^{56,57} Both poorer thermal stability and smaller activation energy is an indication that N self-diffusion in CoN would be significantly higher than that in FeN. Therefore, when CoN samples are deposited even at a moderate temperature like 400 K , N diffuses out leaving behind fcc Co that has

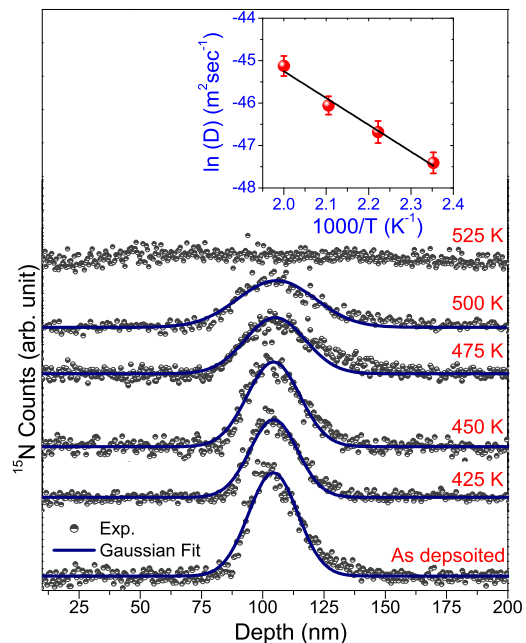


FIG. 15. (Color online) SIMS depth profile of ^{15}N on a Si (substrate)[$\text{Co}^{\text{nat}}\text{N}(100\text{ nm})|\text{Co}^{15}\text{N}(2\text{ nm})|\text{Co}^{\text{nat}}\text{N}(100\text{ nm})$] trilayer after annealing at different temperatures. Inset shows the Arrhenius plot of diffusivity of N.

been often mistaken for Co_4N . High self-diffusion of N in Co-N can also be understood from the fact that the enthalpy of nitride formation in the Co-N system is typically $\sim 0\text{ J/mol}$,³ whereas it is around -47 kJ/mol ²³ in the Fe-N system. This as well explains the poorer thermal stability cobalt nitrides as compared to iron nitrides.

IV. CONCLUSION

In this work, we investigated the pathways to attain a stoichiometric Co_4N phase. This could be achieved when the Co_4N phase emerges from the metallic state of Co target. More importantly, the T_s has an immense role in Co_4N phase formation. Contrary to general assumption, the Co_4N phase can only be formed at $T_s = 300\text{ K}$. Detailed analysis of structure, composition and magnetic properties of Co_4N samples deposited at different T_s reveals that they become N deficient even if the T_s is raised to 400 K . This is an important observation as most of the Co_4N films reported so far were deposited at $T_s > 400\text{ K}$ and the LP of resulting films was more closer to fcc Co rather than Co_4N . We show that stoichiometric polycrystalline and epitaxial Co_4N films can be formed at $T_s = 300\text{ K}$. These results have been explained by measuring N self-diffusion in CoN. We found that N self-diffusion comes out to be orders of magnitude larger than the anticipated value. This explains that while the Fe_4N can be formed at high T_s ($\sim 670\text{ K}$), Co_4N can only be formed at low T_s .

ACKNOWLEDGMENTS

Authors thank the Department of Science and Technology, India (SR/NM/Z-07/2015) for the financial support and Jawaharlal Nehru Centre for Advanced Scientific Research (JNCASR) for managing the project. A part of this work was performed at AMOR, Swiss Spallation Neutron Source, Paul Scherrer Institute, Villigen, Switzerland. We acknowledge help received from L. Behera and Seema in sample preparation and various mea-

surements. M. Horisberger is acknowledged for depositing ^{15}N enriched CoN samples. We are thankful to A. Gome for XRR, V. Ganesan and M. Gangrade for AFM, R. Rawat for resistivity, R. J. Choudhary and M. Tripathi for S-VSM, A. Wadikar for XPS and R. Sah for XAS measurements. We are grateful to A. K. Sinha for support and encouragements.

REFERENCES

- ¹ S. F. Matar, A. Houari, and M. A. Belkhir, *Phys. Rev. B* **75**, 245109 (2007).
- ² Y. Imai, Y. Takahashi, and T. Kumagai, *Journal of Magnetism and Magnetic Materials* **322**, 2665 (2010).
- ³ Y. Imai, M. Sohma, and T. Suemasu, *Journal of Alloys and Compounds* **611**, 440 (2014).
- ⁴ J. M. D. Coey and P. A. I. Smith, *J. Magn. Magn. Mat.* **200**, 405 (1999).
- ⁵ P. Mohn and S. Matar, *Journal of Magnetism and Magnetic Materials* **191**, 234 (1999).
- ⁶ M. Meinert, *Journal of Physics: Condensed Matter* **28**, 056006.
- ⁷ S. Kokado, N. Fujima, K. Harigaya, H. Shimizu, and A. Sakuma, *Physical Review B* **73**, 172410 (2006).
- ⁸ Y. Takahashi, Y. Imai, and T. Kumagai, *Journal of Magnetism and Magnetic Materials* **323**, 2941 (2011).
- ⁹ A. Sakuma, *Journal of magnetism and magnetic materials* **102**, 127 (1991).
- ¹⁰ R. Coehoorn, G. Daalderop, and H. Jansen, *Physical Review B* **48**, 3830 (1993).
- ¹¹ K. Oda, T. Yoshio, and K. Oda, *Journal of Materials Science* **22**, 2729 (1987).
- ¹² C. Silva, A. Vovk, R. da Silva, P. Strichonavec, P. Algarebel, A. Casaca, C. Meneghini, I. Carlomagno, M. Godinho, and M. Cruz, *Journal of Alloys and Compounds* **633**, 470 (2015).
- ¹³ K. Ito, K. Harada, K. Toko, H. Akinaga, and T. Suemasu, *Journal of Crystal Growth* **336**, 40 (2011).
- ¹⁴ K. Ito, K. Kabara, T. Sanai, K. Toko, Y. Imai, M. Tsunoda, and T. Suemasu, *Journal of Applied Physics* **116**, 053912 (2014).
- ¹⁵ C. Silva, A. Vovk, R. da Silva, P. Strichovanec, P. Algarebel, A. Goncalves, R. Borges, M. Godinho, and M. Cruz, *Thin Solid Films* **556**, 125 (2014).
- ¹⁶ X. Wang, H. Jia, W. Zheng, Y. Chen, and S. Feng, *Thin Solid Films* **517**, 4419 (2009).
- ¹⁷ H. Jia, X. Wang, W. Zheng, Y. Chen, and S. Feng, *Materials Science and Engineering: B* **150**, 121 (2008).
- ¹⁸ H. Asahara, T. Migita, T. Tanaka, and K. Kawabata, *Vacuum* **62**, 293 (2001).
- ¹⁹ J.-S. Fang, L.-C. Yang, C.-S. Hsu, G.-S. Chen, Y.-W. Lin, and G.-S. Chen, *Journal of Vacuum Science & Technology A: Vacuum, Surfaces, and Films* **22**, 698 (2004).
- ²⁰ M. Lourenço, M. Carvalho, P. Fonseca, T. Gasche, G. Evans, M. Godinho, and M. Cruz, *Journal of Alloys and Compounds* **612**, 176 (2014).
- ²¹ N. Pandey, M. Gupta, R. Gupta, S. Chakravarty, N. Shukla, and A. Devishvili, *Journal of Alloys and Compounds* **694**, 1209 (2017).
- ²² R. Gupta, N. Pandey, A. Tayal, and M. Gupta, *AIP Advances* **5**, 097131 (2015).
- ²³ F. Tessier, A. Navrotsky, R. Niewa, A. Leineweber, H. Jacobs, S. Kikkawa, M. Takahashi, F. Kanamaru, and F. J. DiSalvo, *Solid State Sciences* **2**, 457 (2000).
- ²⁴ N. Pandey, M. Gupta, R. Gupta, P. Rajput, and J. Stahn, *Journal of Magnetism and Magnetic Materials* **448**, 274 (2018).
- ²⁵ D. M. Phase, M. Gupta, S. Potdar, L. Behera, R. Sah, and A. Gupta, *AIP Conference Proceedings* **1591**, 685 (2014).
- ²⁶ H. Zhang, J. Poole, R. Eller, and M. Keefe, *Journal of Vacuum Science and Technology A* **17** (1999).
- ²⁷ S. Ram, *Materials Science and Engineering: A* **304**, 923 (2001).
- ²⁸ K. Shih and J. Karasinski, *Journal of applied physics* **73**, 8377 (1993).
- ²⁹ W. Diekmann, G. Panzner, and H. Grabke, *Surface Science* **218**, 507 (1989).
- ³⁰ K. Kishi and M. Roberts, *Surface Science* **62**, 252 (1977).
- ³¹ F. Honda and K. Hirokawa, *Talanta* **25**, 383 (1978).
- ³² D. Frost, C. McDowell, and I. Woolsey, *Chemical Physics Letters* **17**, 320 (1972).
- ³³ C. Powell, *Journal of Electron Spectroscopy and Related Phenomena* **185**, 1 (2012).
- ³⁴ B. Ravel and M. Newville, *Journal of Synchrotron Radiation* **12**, 537 (2005).
- ³⁵ K. Ito, K. Harada, K. Toko, M. Ye, A. Kimura, Y. Takeda, Y. Saitoh, H. Akinaga, and T. Suemasu, *Applied Physics Letters* **99**, 252501 (2011).
- ³⁶ K. Ito, K. Toko, Y. Takeda, Y. Saitoh, T. Oguchi, T. Suemasu, and A. Kimura, *Journal of Applied Physics* **117**, 193906 (2015).
- ³⁷ T. I. Morrison, M. B. Brodsky, N. J. Zaluzec, and L. R. Sill, *Phys. Rev. B* **32**, 3107 (1985).
- ³⁸ T. I. Morrison, C. L. Foiles, D. M. Pease, and N. J. Zaluzec, *Phys. Rev. B* **36**, 3739 (1987).
- ³⁹ H. Li, Y. Zhang, K. Yang, H. Liu, X. Zhu, and H. Zhou, *Applied Surface Science* **406**, 110 (2017).
- ⁴⁰ M. Björck and G. Andersson, *Journal of Applied Crystallography* **40**, 1174 (2007).
- ⁴¹ M. Shiga (AIP, 1974) pp. 463–477.
- ⁴² G. W. Wiener and J. A. Berger, *Journal Of Metals* **7**, 360 (1955).
- ⁴³ B. Frazer, *Physical Review* **112**, 751 (1958).

- ⁴⁴ S. Berg, E. Srammar, and T. Nyberg, *Thin Solid Films* **565**, 186 (2014).
- ⁴⁵ S. Berg and T. Nyberg, *Thin solid films* **476**, 215 (2005).
- ⁴⁶ T. Nyberg, S. Berg, U. Helmersson, and K. Hartig, *Applied Physics Letters* **86**, 164106 (2005).
- ⁴⁷ A. Anders, *Journal of Applied Physics* **121**, 171101 (2017).
- ⁴⁸ K. Sarakinos, J. Alami, and S. Konstantinidis, *Surface and Coatings Technology* **204**, 1661 (2010).
- ⁴⁹ T. Kubart, D. H. Trinh, L. Liljeholm, L. Hultman, H. Högberg, T. Nyberg, and S. Berg, *Journal of Vacuum Science & Technology A: Vacuum, Surfaces, and Films* **26**, 565 (2008).
- ⁵⁰ T. Kubart, O. Kappertz, T. Nyberg, and S. Berg, *Thin Solid Films* **515**, 421 (2006).
- ⁵¹ S. Pereira, M. Correia, E. Pereira, K. O'Donnell, E. Alves, A. Sequeira, N. Franco, I. Watson, and C. Deatcher, *Applied physics letters* **80**, 3913 (2002).
- ⁵² W.-X. Ni, K. Lyutovich, J. Alami, C. Tengstedt, M. Bauer, and E. Kasper, *Journal of Crystal Growth* **227-228**, 756 (2001), proceeding of the Eleventh International Conference on Molecular Beam Epitaxy.
- ⁵³ J. L. Costa-Krämer, D. Borsa, J. M. García-Martín, M. S. Martín-González, D. Boerma, and F. Briones, *Physical Review B* **69**, 144402 (2004).
- ⁵⁴ M. B. Stearns and Y. Cheng, *Journal of Applied Physics* **75**, 6894 (1994).
- ⁵⁵ A. Tayal, M. Gupta, N. Lalla, A. Gupta, M. Horisberger, J. Stahn, K. Schlage, and H.-C. Wille, *Physical Review B* **90**, 144412 (2014).
- ⁵⁶ A. Tayal, M. Gupta, A. Gupta, P. Rajput, and J. Stahn, *Physical Review B* **92**, 054109 (2015).
- ⁵⁷ M. Gupta, A. Tayal, A. Gupta, R. Gupta, J. Stahn, M. Horisberger, and A. Wildes, *Journal of Applied Physics* **110**, 123518 (2011).
- ⁵⁸ M. Gupta, A. Gupta, S. Rajagopalan, and A. Tyagi, *Physical Review B* **65**, 214204 (2002).